ACS Catalysis

pubs.acs.org/acscatalysis

Research Article

Steric and Orbital Effects Induced by Isovalent Dopants on the Surface Chemistry of ZrO_2

Farahnaz Maleki and Gianfranco Pacchioni*

Cite This: *ACS Catal.* 2021, 11, 554−567

Read Online

ACCESS | Metrics & More | Article Recommendations | Supporting Information

ABSTRACT: Sometimes, dopants in oxide surfaces are referred to as single-atom catalysts, at least when these species are incorporated in the supporting lattice. Usually, single atom catalysts are transition metal atoms stabilized on an oxide surface, and the activity is due to the valence electrons of these species. However, the surface chemistry can be modified also by the presence of isovalent heteroatoms, where the total number of valence electrons of the active site is the same as for the regular surface. The effect of isovalent dopants on the chemical reactivity of tetragonal ZrO_2 has been studied with first principles calculations. Zr ions in the bulk, subsurface, and surface sites have been replaced with Si, Ge, Sn, Pb, Ti, Hf, and Ce ions. Surface or subsurface sites are clearly preferred. The dopants modify the local structure of the surface and introduce new empty states in the band gap, thus affecting the Lewis acid properties of the surface. We studied the effect of the dopants on the decomposition of HCOOH. This can follow four paths with desorption of (a) H_2, (b) CO, (c) H_2O, or (d) CO_2. On pure ZrO_2 reaction (a) dehydrogenation is preferred followed by decarbonylation (b). Ti, Hf, and Ce have some effect on the decomposition but do not change the order of reactivity. On the contrary, in the presence of Si, decarbonylation becomes the preferred path. If Ge occupies surface sites, reaction (d) loss of CO_2 is by far more favorable. With Sn, dehydrogenation remains energetically preferred but the ordering of the other reactions changes, while Pb makes CO_2 desorption slightly preferred over release of H_2. These effects virtually disappear when the dopants occupy subsurface sites. The study shows that "steric" and/or "orbital" effects of isovalent dopants on a catalyst surface are sufficient to change the reaction products compared to the undoped system.

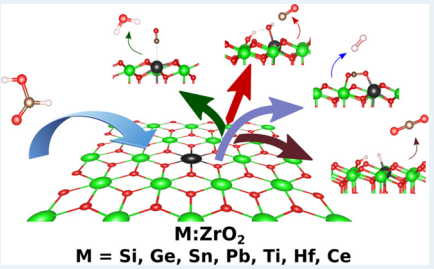

KEYWORDS: *zirconia surface, doping, single atom catalyst, formic acid decomposition, density functional theory*

1. INTRODUCTION

Dopants are used to change the electronic, optical, chemical, and mechanical properties of a material. In catalysis and sensor technologies, dopants are widely used to increase the activity and selectivity or the sensing properties.[1−4] Dopants can also affect the structural stability of a crystalline phase, or facilitate the formation of defects (e.g., oxygen vacancies)[5] that sometimes stabilize a particular polymorph, as for the case of Y-stabilized zirconia.[6,7]

In catalysis, the effect of doping has been studied in various contexts. Metiu and co-workers have studied the oxygen vacancy formation energy in an oxide surface as a measure of how easily lattice oxygen may participate in oxidation reactions, and how this is affected by replacing lattice atoms by other metal dopants.[1,8] Aliovalent dopants have been used to improve the performance of perovskite (ABO_3) surfaces for thermochemical H_2O and CO_2 splitting,[9] or to selectively induce charging of supported metal particles, as for Au on MgO and CaO surfaces.[10]

Bulk doping of zirconia has been studied in the past. ZrO_2 thin films doped with rare elements were prepared by sol−gel giving rise to the formation of tetragonal zirconia with interesting optical properties.[11] Sol−gel has been used also to synthetize Zn-doped ZrO_2 nanoparticles used as substrates for surface-enhanced Raman scattering.[12] In Fe-doped ZrO_2 nanocrystals, the magnetic behavior critically depends on the dopant concentration.[13] Ti-doped ZrO_2 has been investigated as potential nanophosphor.[14] Ce-doped[15] and Al-doped[16] ZrO_2 nanostructures have been investigated for their optical properties. This brief list demonstrates the potential connected to the incorporation of doping elements in bulk zirconia, which in the case of aliovalent dopants may lead to compensating defects, cation or anion vacancies, trapped holes or electrons, etc. to maintain charge neutrality.[17]

Things are different when dopants are on the surface. In the last years, the notion of single-atom catalyst (SAC) has been introduced to identify isolated atomic species stabilized on a support.[18] However, when the active species is intimately bound to the surface, for instance by replacing a lattice ion, the concept of dopant and SAC coincide. SACs are not static entities, and often their structure evolves as a function of the

Received: October 21, 2020
Revised: December 12, 2020
Published: December 28, 2020

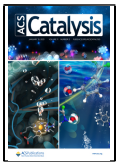

https://dx.doi.org/10.1021/acscatal.0c04553
ACS Catal. 2021, 11, 554−567

external conditions. For instance, Pt atoms on TiO_2 are initially incorporated in the lattice replacing Ti ions (Pt dopants) and then evolve into surface species stabilized by extra O atoms or OH groups.[19] SACs usually consist of a transition metal atom stabilized on a support. The valence electrons of this atom make it an active catalytic site. However, other effects also contribute to the activity of the heteroatom, not related to the number of valence electrons.

To show this, we have considered the surface of tetragonal ZrO_2 and we have replaced systematically the surface Zr ions with isovalent dopants. Zr ions at the surface, subsurface, and bulk have been replaced by a series of atoms with the same valency: Si, Ge, Sn, Pb, Ti, Hf, and Ce. The scope is to analyze the impact of isovalent doping on the surface chemistry of the oxide. To this end, we have considered the interaction of the zirconia surface with formic acid, HCOOH. This species is particularly relevant since in the process of CO_2 reduction and conversion to methanol one of the reaction paths implies that CO_2 primarily hydrogenates to $HCOO^-$ and then to HCOOH before it leads to CH_3OH. This process has been studied for instance on tetragonal $ZrO_2(101)$-supported copper nanowires[20] or on Pd catalysts loaded on ZrO_2.[21] In a recent study, methanol synthesis via CO_2 hydrogenation has been investigated on $ZrO_2/CuO_2/Cu(111)$ catalysts, showing the promotional effects of small ZrO_2 particles.[22] The synthesis of HCOOH from CO_2 on $Fe_xZr_{1-x}O_2$ has also been reported showing the important role of the Fe dopant.[23]

The opposite reaction, the decomposition of formic acid with formation of carbon dioxide and hydrogen ($HCOOH \rightarrow CO_2 + H_2$), is also of interest and has been studied on several metals (Pt, Pd, Ni, Cu, Rh, and Au) and metal oxides (TiO_2, MgO, ZnO, NiO, MgO, and V_2O_5)[24−28] including ZrO_2.[29] This incomplete list of literature data shows the importance of the interaction of formic acid with solid surfaces and the complexity of the reactions involved.

In the following study we report the results from first principles calculations on the structural, electronic, and chemical changes induced by a series of tetravalent dopants on the $ZrO_2(101)$ surface. The scope is to show that the presence of isovalent species incorporated in the surface layer, while not altering the total number of electrons available for the chemical reactions, may have profound effects on the surface chemistry due to either "steric" effects connected to the size of the dopants, or "orbital" effects connected to the different energies and different tendencies to form hybrid orbitals of the atomic orbitals of the heteroatom.

The paper is organized as follows. After a Computational section, we present the structural and electronic effects of doping ZrO_2, with particular emphasis on the preferred sites and the modification of the electronic band gap. The rest of the paper presents the results of the adsorption properties of HCOOH, and of CO_2, CO, H_2O, and H_2 on pure and doped ZrO_2. The following section discusses the thermodynamics of the decomposition process of HCOOH, comparing with the bare doped surface. Potential effects of the dopants on the kinetics of the decomposition processes are also addressed. Finally, some general conclusions are summarized in the last section.

2. COMPUTATIONAL DETAILS

Density functional theory (DFT) calculations have been performed using the Vienna Ab Initio Simulation Package (VASP 5.4.4).[30−32] The generalized gradient approximations (GGAs) have been adopted for the exchange−correlation functional within the Perdew−Burke−Ernzerhof (PBE) formulation.[33] To partially correct the self-interaction error, the PBE + U[34,35] approach has been adopted. Here, we set the Hubbard parameter to $U = 3$ eV for the 3d states of Ti,[36] $U = 4$ eV for the 4d states of Zr,[37] and $U = 1$ eV for the 5d states of Hf;[38] $U = 4$ eV has been used for the Ce 4f states.[39] Of course, one should be aware of the fact that the DFT + U approach is not free from limitations, in particular when used to study catalytic processes as the results may depend in part on the choice of the U parameter.[40] The D3 dispersion energy was included by means of the Becke−Johnson damping approach.[41,42] To describe the effect of the core electrons, the projector augmented wave (PAW) method[43,44] was used where H (1s), C (2 s, 2p), O (2s, 2p), Si (3s, 3p), Ge (4s, 4p), Sn (5s, 5p), Pb (6s, 6p), Ti (3s, 4s, 3p, 3d), Zr (4s, 5s, 4p, 4d), Hf (5s, 6s, 5p, 5d), and Ce (5s, 6s, 5p, 4f, 5d) were considered as valence electrons and therefore treated explicitly. The energy basis cutoff was set to 400 eV, and the optimizations were performed using the conjugate gradient scheme until the change in total energy between successive steps was less than 10^{-5} eV.

We described the tetragonal zirconia surface, t-ZrO_2 (101), with a 3 × 2 supercell with 5 layers of Zr and 10 layers of O (5 ZrO_2 trilayers).[45] The supercell thus has a composition $Zr_{60}O_{120}$ and the dopant concentration is 1.67%. The sampling of the reciprocal space is set to the Γ-point. The slabs were separated by more than 10 Å of vacuum.

Theoretical simulations of solid materials and surfaces can be done either using the experimental or the fully optimized lattice parameters. While in general the results should be similar, for zirconia in some specific cases different reaction energies are obtained with the two approaches. Experience in our group has shown that it is recommended to use the optimized lattice parameters. Here, we used both experimental and optimal lattice constants for comparison, but we discuss in the paper only the results obtained from fully optimized bulk lattice parameters. This has been done using a kinetic energy cutoff of 600 eV and a 8 × 8 × 8 Monkhorst−Pack k-point grid; the resulting parameters were then used for the optimization of the atomic positions in the slab models. In both cases, fixed or optimized lattice constants, all atoms were allowed to move during geometry optimization. Atoms were allowed to change their positions until ionic forces were smaller than |0.01| eV/Å.

The adsorption energies were calculated according to the following equation:

$$E_{ads} = E(x/\mathrm{M}\text{:}\ ZrO_2) - E(x)(g) - E(\mathrm{M}\text{:}\ ZrO_2) \qquad (1)$$

where x is the adsorbed molecule (H_2O, CO, CO_2, H_2, and HCOOH) and M = Si, Ge, Sn, Pb, Ti, Hf, and Ce. Vibrational frequencies are calculated within the harmonic approximation via the diagonalization of the dynamical matrix. The active fragment for the ionic displacements is restricted to the adsorbed molecules and the surface ions directly taking part in the adsorption process.

To determine the transition state, we used the nudged elastic band (NEB) method.[46] The images were optimized to obtain the minimum energy path until forces on ions were smaller than |0.05| eV/Å. Finally, atomic charges have been determined using the Bader analysis.

https://dx.doi.org/10.1021/acscatal.0c04553
ACS Catal. 2021, 11, 554−567

3. STRUCTURAL AND ELECTRONIC PROPRETIES OF M:ZRO$_2$

3.1. Stability and Coordination. The seven dopants considered have been incorporated in three different substitutional positions, always replacing a lattice Zr^{4+} ion: (a) surface, (b) subsurface (second layer of our slab), and (c) bulk (most internal layer of the slab model). The results are summarized in a graphic way in Figure 1 where the preferred positions of the various dopants is shown. First, we notice that in no circumstance the dopants want to occupy internal (bulk) layer positions; they all prefer surface or subsurface sites. In particular, Si, Sn, Ce, and Pb prefer to replace Zr ions at the surface, while Ti, Ge, and Hf prefer to go to the subsurface.

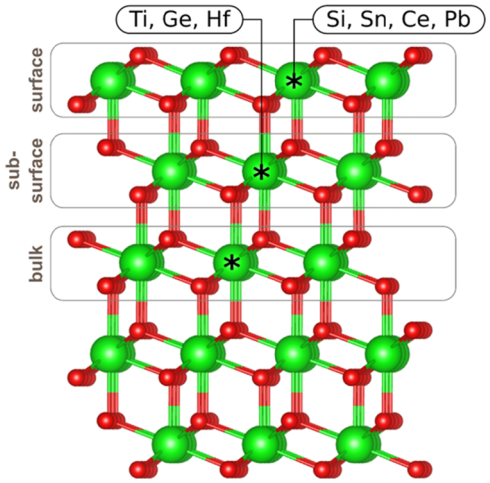

Figure 1. Preferred position of various dopants on a ZrO_2 slab.

This can be attributed to the fact that the replacement of Zr with cations which are smaller or larger in size induces a local geometrical relaxation. Even the coordination number is different: some dopants such as Si and Ge strongly prefer to form pseudotetrahedral structures, Si_{4c} and Ge_{4c}, while big ions such as Sn, Pb, or Ce can coordinate up to eight O atoms, Table 1. The resulting strain is accommodated more easily on the surface layers, which is the reason for the tendency to occupy these sites. In some cases, such as Ce and Pb, the difference between the two sites, surface or subsurface, is very large, being of 0.7−1.0 eV, and in favor of the top layer, Table 1. Ge and Ti exhibit a preference for subsurface sites, with a ΔE of 0.18 and 0.25 eV, respectively. In the case of Hf the preference for the subsurface is tiny, less than 0.1 eV and one cannot exclude that both sites are occupied at thermal equilibrium. In Table 1, we report the relative stabilities also for a set of calculations where the lattice parameters are taken from the experiment, see ΔE(exp). The results are qualitatively similar, but the energy differences may differ significantly in some cases.

In general, the preference for surface or subsurface layers suggests that thermal annealing can induce segregation of the dopants toward the surface of the ZrO_2 nanoparticles, where they will locally modify the surface chemistry.

The preference for surface or subsurface sites can be partly rationalized with the sizes of the various dopants considered. The ionic radius however depends on the coordination of an ion in a crystal, and we have seen that the various dopants assume different coordination numbers when incorporated in ZrO_2. Figure 2 shows the cation sizes as a function of the atomic number, where the values refer to 4c ions for the case of Si and Ge, and 6c ions for the other dopants (see also Table S1 in Supporting Information). Ce and Pb, the largest ions, prefer

Table 1. Difference in Stability (ΔE, eV) for Various Dopants at Surface, Subsurface, and Bulk Positions Computed for Fully Optimized (Opt) or Fixed Experimental (Exp) Lattice Constants, Value of Optimized Lattice Constants (a, b, c, Å), Dopant Coordination Number (c.n.), Bader Charge (Q|e|), Computed Band Gap (E_g, eV), and Work Function (Φ, eV)

	ΔE(opt)	ΔE(exp)	a^a	b^a	c^a	c.n.	q	E_g	Φ
ZrO_2			10.77	12.42	13.95	Zr_{7c}	2.73	4.12	6.62
Si:ZrO_2 (surf)	0.000	0.000	10.75	12.40	14.07	Si_{4c}	3.10	3.77	6.60
Si:ZrO_2 (sub_surf)	0.330	0.543	10.72	12.37	14.15	Si_{4c}	3.11	4.27	6.52
Si:ZrO_2 (bulk)	0.454	0.633	10.73	12.38	14.11	Si_{4c}	3.11	4.21	6.55
Ge:ZrO_2 (surf)	0.180	0.480	10.81	12.36	13.99	Ge_{5c}	2.16	3.87	6.48
Ge:ZrO_2 (sub_surf)	0.000	0.000	10.75	12.41	14.02	Ge_{4c}	2.18	4.25	6.53
Ge:ZrO_2 (bulk)	0.087	0.064	10.76	12.41	14.00	Ge_{4c}	2.19	4.23	6.58
Sn:ZrO_2 (surf)	0.000	0.000	10.76	12.41	13.97	Sn_{7c}	2.21	4.15	6.59
Sn:ZrO_2 (sub_surf)	0.215	0.121	10.76	12.41	13.96	Sn_{8c}	2.31	4.16	6.55
Sn:ZrO_2 (bulk)	0.247	0.151	10.76	12.41	13.97	Sn_{8c}	2.31	4.16	6.56
Pb:ZrO_2 (surf)	0.000	0.000	10.77	12.42	13.97	Pb_{7c}	1.76	4.23	6.56
Pb:ZrO_2 (sub_surf)	0.669	0.725	10.77	12.42	13.96	Pb_{8c}	1.89	4.22	6.56
Pb:ZrO_2 (bulk)	0.672	0.729	10.77	12.42	13.97	Pb_{8c}	1.87	4.23	6.58
Ti:ZrO_2 (surf)	0.245	0.105	10.77	12.40	13.95	Ti_{6c}	2.32	3.87	6.51
Ti:ZrO_2 (sub_surf)	0.000	0.000	10.75	12.40	13.97	Ti_{7c}	2.34	3.77	6.70
Ti:ZrO_2 (bulk)	0.068	0.072	10.75	12.40	13.97	Ti_{7c}	2.34	3.72	6.71
Hf:ZrO_2 (surf)	0.098	0.140	10.76	12.41	13.95	Hf_{7c}	2.64	4.12	6.52
Hf:ZrO_2 (sub_surf)	0.000	0.000	10.77	12.41	13.94	Hf_{8c}	2.64	4.12	6.52
Hf:ZrO_2 (bulk)	0.016	0.025	10.76	12.41	13.94	Hf_{8c}	2.63	4.12	6.56
Ce:ZrO_2 (surf)	0.000	0.000	10.78	12.43	13.95	Ce_{7c}	2.39	4.15	6.50
Ce:ZrO_2 (sub_surf)	0.860	0.948	10.77	12.42	13.96	Ce_{8c}	2.41	4.14	6.62
Ce:ZrO_2 (bulk)	0.807	0.889	10.77	12.42	13.97	Ce_{8c}	2.42	4.14	6.62

[a]The experimental lattice constants are 10.99, 12.75, and 13.52 Å.

https://dx.doi.org/10.1021/acscatal.0c04553
ACS Catal. 2021, 11, 554−567

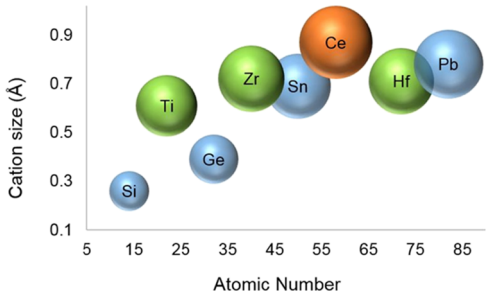

Figure 2. Cation size versus the atomic number for M^{4+} ions: 4c (M = Si and Ge) and 6c (M = Sn, Pb, Ti, Zr, Hf, and Ce).

to stay on the surface to reduce steric repulsion. Ti and Hf have comparable cation sizes and can easily replace Zr in subsurface sites. The same is true for Ge, but not for Si which is too small, and gives rise to local rearrangements that occur more easily on the top layer, where there are less constraints. Table 1 also shows the values of the optimized lattice parameters; however, these do not change very much compared to pure ZrO_2. This is due to the fact that we are considering a low level of doping (<2%).

3.2. Electronic Effects. The presence of the dopants can affect the extent and the nature of the gap in ZrO_2 and can result in new electronic states in the band gap. Given the low level of doping considered, if new states appear in the gap these will be localized and will not give rise to the formation of a band. Some effects on the band edges can arise from the structural relaxations induced by the incorporation of the heteroatoms. Table 1 shows the values of the computed band gap in pure and doped zirconia, as well as the work function Φ which corresponds to the position of the top of the valence band (VB) with respect to the vacuum level. Since the calculations have been done at the DFT + *U* level, the computed band gap for ZrO_2, 4.12 eV, is considerably underestimated (the experimental values are between 5 and 5.8 eV).[47] However, the focus here is on the changes induced by the dopants and not on the absolute values.

The results are reported in Table 1 and in Figure 3 (for the density of states, see Figure S1 in Supporting Information). Si, which prefers to occupy surface sites, induces a reduction of the band gap by 0.35 eV but does not introduce new states in the gap, Figure 3a; notice that if Si is on the subsurface the effect on the band gap is small and in the opposite direction, Figure 3b. Ge has a similar effect on the gap, but it also introduces new shallow empty states due to Ge 4d orbitals just below the conduction band (CB). This effect is even more pronounced in Sn. While the edges of the VB and CB do not change compared to pure ZrO_2, Sn introduces new acceptor 5d states deep in the gap. These states can trap electrons from donor species and change the Lewis acidity of the surface. The presence of acceptor states in the gap becomes even more

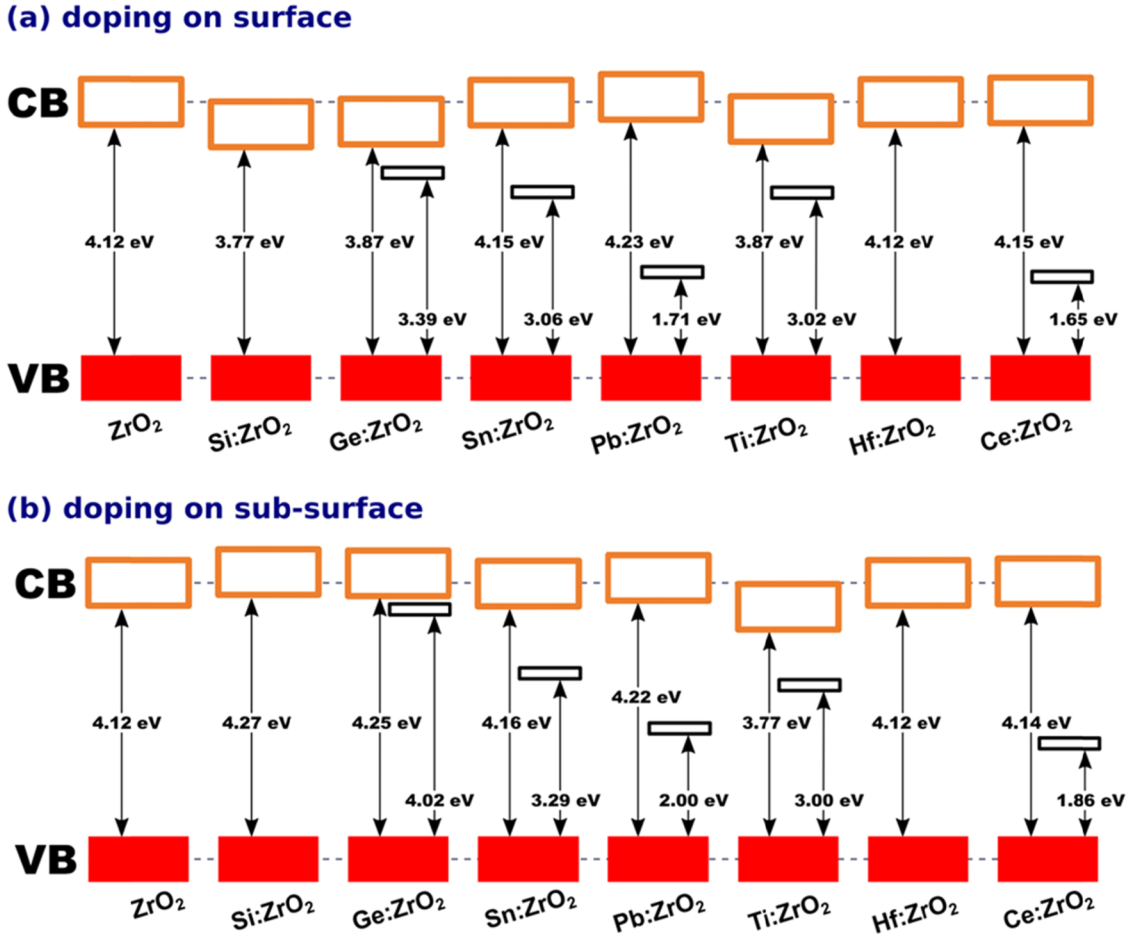

Figure 3. Schematic representation of VB and CB edges, band gaps, and defect states in the gap in pristine and doped ZrO_2 surfaces. (a) Dopants at the surface; (b) dopants at subsurface positions.

https://dx.doi.org/10.1021/acscatal.0c04553
ACS Catal. 2021, 11, 554−567

dramatic with Pb, since the empty 6d levels are now only 1.7−2 eV above the VB.

As for Si, Ti also has the effect to reduce the band gap, independent of the site occupied, but differently from Si, Ti introduces empty 3d states that are lower in energy than the Zr 4d states that contribute to the CB. This is no longer the case if one considers the third member of the series, Hf, whose empty 5d orbitals are above the bottom of the CB so that no new states appear in the gap due to this dopant. When Hf replaces Zr, actually no change is observed in the gap. The last cation considered is Ce^{4+} which has 4f empty states low in energy and close to the top of the VB, Figure 3. This is consistent with a recent combined electron paramagnetic resonance (EPR) and DFT study of Ce-doped ZrO_2.[48]

The other property considered is the work function Φ, Table 1, which in ZrO_2 is 6.62 eV. The results show very little change of this quantity, which goes from 6.48 eV in Ge:ZrO_2 to 6.71 in Ti:ZrO_2. One can conclude that the basicity of the surface, as measured by the position of the filled O 2p states, is not significantly affected by doping, at variance with the acid properties which are related to the presence of new empty levels.

Finally, a few comments on the local charge of the cation dopant, as measured by the Bader analysis. In ZrO_2, Zr has a charge q = 2.73 |el|; the doping elements considered have charges that are bigger or smaller than the host, with Si exhibiting the largest value, q = 3.11 |el|, and Pb the smallest, q = 1.76 |el|. Some ions have virtually the same charge as Zr, see for instance Hf, q = 2.64 |el|, Table 1.

To summarize, one can identify two contributions to a modified surface reactivity. The first one is purely structural, due to the different sizes of the heteroatoms and their tendency to assume specific coordination environments (e.g., to take a tetrahedral coordination in the case of Si and Ge); the other effect is related to the presence of new atomic orbitals associated with the dopant, which can result in empty states in the gap or in the possibility to mix these orbitals with those of the surrounding or of incoming species. Even keeping the total electron density available for surface chemical reactions constant, these two effects have the potential to deeply modify the surface reactivity, as it will be shown in the following sections.

4. ADSORPTION PROPERTIES OF M:ZRO$_2$

In the gas-phase formic acid, HCOOH, can decompose either by dehydrogenation or by dehydration; both reactions are endothermic, but dehydrogenation has a lower energy cost, which according to our DFT calculations amounts to 0.25 eV, to be compared with the 0.93 eV cost associated to the dehydration reaction:

$$\mathrm{HCOOH\ (g)} \rightarrow \mathrm{CO_2\ (g)} + \mathrm{H_2\ (g)}\ \Delta E = +0.25\ \mathrm{eV\ (dehydrogenation)} \quad (2)$$

$$\mathrm{HCOOH\ (g)} \rightarrow \mathrm{CO\ (g)} + \mathrm{H_2O\ (g)}\ \Delta E = +0.93\ \mathrm{eV\ (dehydration)} \quad (3)$$

On the surface of a solid catalyst, decarbonylation can also occur via CO or CO_2 desorption, giving rise to four competing reactions:

$$\mathrm{HCOOH\ (g)} + \mathrm{M{:}\ ZrO_2} \rightarrow \mathrm{H_2\ (g)} + \mathrm{CO_{2(ads)}/M{:}\ ZrO_2}\ \Delta E_R\ (\mathrm{H_2}) \quad (4)$$

$$\mathrm{HCOOH\ (g)} + \mathrm{M{:}\ ZrO_2} \rightarrow \mathrm{H_2O\ (g)} + \mathrm{CO_{(ads)}/M{:}\ ZrO_2}\ \Delta E_R\ (\mathrm{H_2O}) \quad (5)$$

$$\mathrm{HCOOH\ (g)} + \mathrm{M{:}\ ZrO_2} \rightarrow \mathrm{CO\ (g)} + \mathrm{H_2O_{(ads)}/M{:}\ ZrO_2}\ \Delta E_R\ (\mathrm{CO}) \quad (6)$$

$$\mathrm{HCOOH\ (g)} + \mathrm{M{:}\ ZrO_2} \rightarrow \mathrm{CO_2\ (g)} + \mathrm{H_{2(ads)}/M{:}\ ZrO_2}\ \Delta E_R\ (\mathrm{CO_2}) \quad (7)$$

On the ZrO_2 surface, formic acid can thus decompose releasing in the gas-phase (a) H_2, leaving an adsorbed CO_2 molecule (b), generating H_2O which desorbs while CO remains bound to the surface, (c) forming gas-phase CO, with formation of an adsorbed H_2O molecule, or (d) desorbing CO_2 with formation of a hydroxylated surface. In the following sections we will analyze the adsorption properties of HCOOH and of the four fragments, CO_2, CO, H_2O, and H_2, resulting from the decomposition before to address the energetics of the processes 4−7 as a function of doping.

4.1. HCOOH Adsorption. In this section we consider the adsorption of formic acid on the (101) t-ZrO_2 surface and its dependence on the presence of dopants. For an overview of adsorption modes of carboxylic acids on ZrO_2 see ref.[49,50] Figure 4 shows four isomers of HCOOH on the pristine

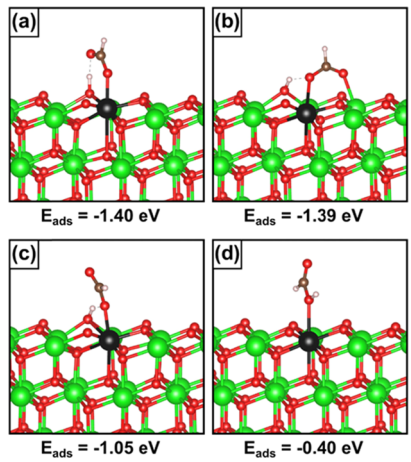

Figure 4. Structure and adsorption energy of four isomers of formic acid on pristine and doped ZrO_2. The structures shown refer to undoped ZrO_2; the position of the dopant for M:ZrO_2 cases corresponds to the black atom.

surface. The first one, monodentate, forms via interaction of the C═O group with a surface cation, while the acid proton of HCOOH is transferred to a surface O ion, Figure 4a. This isomer, bound by −1.40 eV, Table 2, is practically isoenergetic with a bidentate structure where the $HCOO^-$ fragment binds to two surface Zr ions, while the proton is transferred to the surface, Figure 4b. In both isomers, a hydrogen bond forms between the $HCOO^-$ unit and the surface proton.

Two other possible isomers have been considered, Figure 4c,d. The first is a monodentate structure where one of the O atoms of $HCOO^-$ points toward the vacuum, resulting in a

https://dx.doi.org/10.1021/acscatal.0c04553
ACS Catal. 2021, 11, 554−567

Table 2. Adsorption Energy (E_{ads}, eV), Hydrogen-Bond Distance ($R_{O...H}$, Å), and Bond Angle of Adsorbed Formic Acid (∠, °) on Pristine and Doped ZrO_2 Surfaces

		monodentate (Figure 4a)				bidentate (Figure 4b)			
HCOOH		E_{ads}	$R_{O...H}$	∠MOC	∠OCO	E_{ads}	$R_{O...H}$	∠MOC	∠OCO
	ZrO_2	−1.40	1.494	141.7	126.0	−1.39	1.845	130.3	128.0
surface	$Si:ZrO_2$	−1.41	1.577	153.2	126.9	unstable	-	-	-
	$Ge:ZrO_2$	−1.71	1.551	140.2	129.1	−1.68	1.855	123.5	129.6
	$Sn:ZrO_2$	−1.31	1.500	144.2	128.8	−1.46	1.851	125.0	129.5
	$Pb:ZrO_2$	−1.26	1.484	131.8	129.4	−1.23	1.916	123.8	129.9
	$Ti:ZrO_2$	−1.67	1.604	162.8	125.4	−1.80	1.754	129.2	128.8
	$Hf:ZrO_2$	−1.38	1.522	146.1	125.9	−1.48	1.808	130.6	128.1
	$Ce:ZrO_2$	−1.23	1.419	139.3	125.6	−1.28	1.999	131.5	127.2
subsurface	$Si:ZrO_2$	−0.87	1.305	135.9	125.6	−0.60	1.731	133.8	127.7
	$Ge:ZrO_2$	−0.93	1.350	137.2	125.7	−0.75	1.748	133.0	127.8
	$Sn:ZrO_2$	−1.57	1.525	143.5	126.1	−1.62	1.899	128.9	128.4
	$Pb:ZrO_2$	−1.45	1.514	143.9	126.1	−1.58	1.885	129.4	128.2
	$Ti:ZrO_2$	−1.69	1.519	143.1	126.1	−1.28	1.838	131.2	127.8
	$Hf:ZrO_2$	−1.43	1.501	142.0	126.0	−1.41	1.880	129.3	128.2
	$Ce:ZrO_2$	−1.45	1.509	142.8	126.0	−1.51	1.850	131.0	128.1

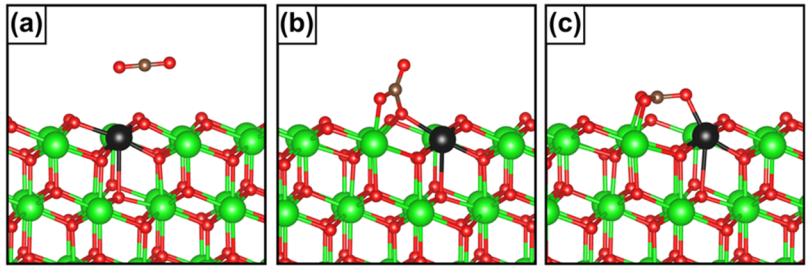

Figure 5. Isomers of CO_2 adsorbed on pristine and doped t-ZrO_2: (a) physisorption, (b) surface carbonate where the CO_3^{2-} complex is "normal" to the surface, and (c) surface carbonate where the CO_3^{2-} complex is "parallel" to the surface.

weaker adsorption energy, −1.05 eV; the other is an undissociated HCOOH molecule, which is only weakly bound, −0.40 eV. Given the large difference in energy, only the two most stable isomers, monodentate and bidentate, have been considered for the study of the dopant effect, Table 2.

The presence of surface dopants does not change in a dramatic way the relative stability of the mono- and bidentate isomers, Table 2. The results are presented as graphs in Figure S2. In some cases, the adsorption is reinforced, for instance for Ti where E_{ads} for the two isomers becomes −1.67 and − 1.80 eV, respectively; in other cases, it is weakened, see, e.g., Pb and Ce where the adsorption energies become −1.2/−1.3 eV. In general, the two isomers remain very close in energy, Table 2. For Ge the binding of HCOOH is strong enough that the dopant becomes more stable in surface position, while without adsorbate it prefers the subsurface site. This is due to the relatively small energy difference between the two sites, 0.18 eV, Table 1; however, in order to migrate from the subsurface to the surface, the Ge atom has to overcome an energy barrier. It is unlikely that the adsorption releases sufficient heat to promote this migration.

More pronounced is the effect of the dopants in subsurface positions. Si and Ge result in a reduction of the adsorption energy and clearly favor the monodentate isomer, Table 2. Ti has the effect to reverse the order of stability of the two isomers compared to the case where it replaces Zr in the top layer: E_{ads} becomes −1.69 eV for the monodentate, and − 1.28 eV for the bidentate species. Notice that when dopants are in the subsurface layer only structural effects become relevant for the reactivity of the surface.

The dopants that reduce the strength of the adsorption of HCOOH have virtually no effect on the chemistry of the surface but those that reinforce the adsorption will have a prominent role in determining the surface reactivity. This is the case in particular of Ti that prefers to occupy subsurface sites and that makes one species, monodentate, more favorable than the other. It is interesting to note that Hf, which belongs to the same group of Zr, has virtually no effect, as $Hf:ZrO_2$ behaves essentially as pure ZrO_2.

In Figure S3a, we present the E_{ads} values for the monodentate form of adsorbed formate, Figure 4a, versus the length of the hydrogen bond formed between the surface proton (OH group) and the O atom of the monodentate moiety; R^2 = 0.80 indicates the existence of some correlation, although other terms also contribute to the adsorption energy, due to the interaction of the $HCOO^-$ fragment with the surface cation. A better correlation (R^2 = 0.95, Figure S3b) is found when one plots E_{ads} versus the length of the hydrogen bond for the bidentate isomer, Figure 4b. Here, the only contribution to the strength of the adsorption comes from the position of the O ion where the proton is bound, which, in turn, depends on the presence of the subsurface dopant.

4.2. CO_2 Adsorption. We consider now the adsorption properties of CO_2, one product of reaction 4, dehydrogenation. The nature of the bonding of CO_2 to undoped t-ZrO_2 has been studied by our group in the past with a similar theoretical approach but using the experimental lattice constants to

https://dx.doi.org/10.1021/acscatal.0c04553
ACS Catal. 2021, 11, 554−567

Table 3. Adsorption Energy (E_{ads}, eV), of Three Isomers of CO_2 Adsorbed on Pristine and Doped ZrO_2

CO_2		physisorbed CO_2(Figure 5a)	"normal" carbonate(Figure 5b)	"parallel" carbonate(Figure 5c)
	ZrO_2	−0.25	unstable	−1.07
surface	Si:ZrO_2	−0.31	unstable	−0.76
	Ge:ZrO_2	−0.32	−0.36	−1.29
	Sn:ZrO_2	−0.22	−0.44	−1.06
	Pb:ZrO_2	−0.24	−0.44	−0.79
	Ti:ZrO_2	−0.28	−0.68	−1.46
	Hf:ZrO_2	−0.21	−0.58	−1.20
	Ce:ZrO_2	−0.32	−0.42	−0.46
subsurface	Si:ZrO_2	−0.27	−0.71	−0.95
	Ge:ZrO_2	−0.28	−0.75	−0.85
	Sn:ZrO_2	−0.26	−0.66	−1.14
	Pb:ZrO_2	−0.25	−0.59	−1.19
	Ti:ZrO_2	−0.26	−0.63	−1.05
	Hf:ZrO_2	−0.24	−0.56	−1.03
	Ce:ZrO_2	−0.25	−0.54	−1.21

construct the slab model of the surface.[51] Further studies have shown that the model of the surface is slightly strained when the experimental lattice constants are used and that this can result in enhanced surface reactivity.[52] Therefore, the present results are obtained using the optimized lattice constants, as for HCOOH adsorption discussed in the previous section.

There are three main adsorption modes of CO_2 on the (101) ZrO_2 surface, Figure 5a−c, physisorption, surface carbonate where the CO_3^{2-} complex is "normal" to the surface, and surface carbonate where the CO_3^{2-} complex is "parallel" to the surface. In this latter case one surface O ion is extracted from the surface to form a CO_3^{2-} unit that interacts with three surface cations, Figure 5c.

Not surprisingly, physisorbed CO_2, bound by −0.25 eV on the undoped surface, Table 3, is barely affected by the replacement of Zr with other ions. A moderate reduction is found for the case of Hf, −0.21 eV, and a small increase (in absolute value) for Ge and Ce, −0.32 eV. The effect is negligible when the dopants are in subsurface positions, Table 3.

More interesting is the case of the "normal" surface carbonate, Figure 5b and Table 3. This isomer is not a local minimum on the surface of clean ZrO_2, while the replacement of Zr with one of the dopants results in a metastable structure (the only exception is Si for which no minimum is found). If the surface Zr ion is replaced by Ti, the "normal" CO_3^{2-} isomer is bound by −0.68 eV, a relatively strong bond. Only slightly smaller is the binding in the case of Hf doping. The results are presented as graphs in Figure S4.

Quite interesting, when the dopants are in subsurface positions, the normal carbonate isomer is always a local minimum, and the binding energy can go up to −0.71 eV (Si) or − 0.75 eV (Ge), Table 3 and Figure S4. Clearly, the perturbation induced by a subsurface cation on the surface O ion that interacts directly with the C atom of the CO_2 molecule is important. Stated differently, subsurface dopants make the surface O ion more reactive toward CO_2, thus increasing the basic character of the surface. Since Ge, Ti, and Hf prefer to go subsurface, their effect can be precisely that to change locally the reactivity of specific O ions, increasing the affinity for CO_2. This is an important observation because the "normal" carbonate is the precursor state of the most stable isomer, the "parallel" carbonate, which is the ground state in all cases considered, Table 3.

4.3. CO Adsorption. CO is produced in the decomposition reaction 5. Compared to CO_2, the interaction of CO with the surface is much simpler since only molecular adsorption occurs, due to the very strong C−O bond. The molecule adsorbs on a surface cation (either Zr^{4+} or the M^{4+} dopant) with the molecular axis normal to the surface. On the pristine surface the bonding to Zr^{4+} has an adsorption energy of −0.42 eV; the CO molecule exhibits a stretching frequency that is blue-shifted by +10 cm^{-1} due to the interaction with the surface electric field; the value is underestimated compared to the experiment where $\Delta\nu$ is +51 cm^{-1},[53] but the use of hybrid functionals is expected to result in closer agreement with the experiment.[54]

Replacing a surface Zr ion with one of the dopants results in some cases in a stronger interaction (in particular for Ti and Ge where E_{ads} is −0.7/−0.8 eV) while in other cases this leads to a weaker bond (Sn and Pb in particular, Table 4). The effect on the vibrational shift is small and can result in a more pronounced blue shift by 8−9 cm^{-1}. An exception is Ce^{4+}: here CO is bound by −0.38 eV, as on the pristine surface, but the CO frequency is shifted by +27 cm^{-1}. The results are summarized in Figure S5. For comparison, shifts up to 33 cm^{-1}

Table 4. Adsorption Energy (E_{ads}, eV), C−O Stretching Frequency (ν, cm^{-1}), Frequency Shift, $\Delta\nu$, and Bond Lengths (R, Å) of CO Adsorbed on Pristine and Doped ZrO_2

CO		E_{ads}	ν_{CO}	$\Delta\nu_{CO}$	R_{CO}	R_{M-C}
	ZrO_2	−0.42	2133	10	1.142	2.519
surface	Si:ZrO_2	−0.52	2142	19	1.141	2.083
	Ge:ZrO_2	−0.80	2138	15	1.142	2.115
	Sn:ZrO_2	−0.23	2130	7	1.142	2.642
	Pb:ZrO_2	−0.25	2141	18	1.141	2.874
	Ti:ZrO_2	−0.66	2121	−2	1.144	2.276
	Hf:ZrO_2	−0.36	2125	2	1.143	2.437
	Ce:ZrO_2	−0.38	2150	27	1.140	2.892
subsurface	Si:ZrO_2	−0.27	2122	−1	1.143	2.635
	Ge:ZrO_2	−0.27	2121	−2	1.143	2.632
	Sn:ZrO_2	−0.38	2131	8	1.142	2.542
	Pb:ZrO_2	−0.43	2133	10	1.142	2.521
	Ti:ZrO_2	−0.37	2131	8	1.142	2.548
	Hf:ZrO_2	−0.41	2132	9	1.142	2.523
	Ce:ZrO_2	−0.44	2133	10	1.142	2.520

https://dx.doi.org/10.1021/acscatal.0c04553
ACS Catal. 2021, 11, 554−567

Table 5. Adsorption Energy (E_{ads}, eV) of Molecular (mol) and Dissociative (diss) Adsorption and Selected Bond Distances (R, Å) and Bond Angles of H_2O Dissociative Adsorption on Pristine and Doped ZrO_2 Surfaces

H_2O		E_{ads} (mol)	E_{ads} (diss)	$R_{O1\text{-}H1}$	$R_{O2\text{-}H2}$	$R_{O2\ldots H1}$	$R_{O3\ldots H2}$	$R_{M\text{-}O2}$	∠MO2H2
	ZrO_2	−0.81	−1.01	1.008	0.969	1.606	2.805	2.078	125.3
surface	Si:ZrO_2	unstable	−1.78	0.999	0.996	1.732	1.800	1.668	105.6
	Ge:ZrO_2	unstable	−2.09	0.999	0.997	1.734	1.823	1.815	100.7
	Sn:ZrO_2	unstable	−1.36	1.011	0.977	1.606	2.371	2.033	104.7
	Pb:ZrO_2	−0.70	−1.03	1.005	0.980	1.657	2.487	2.158	101.7
	Ti:ZrO_2	unstable	−1.67	0.999	1.000	1.710	1.771	1.872	103.3
	Hf:ZrO_2	unstable	−1.16	1.009	0.969	1.600	2.640	2.025	123.0
	Ce:ZrO_2	−0.75	−0.60	1.013	0.971	1.637	3.153	2.253	134.6
subsurface	Si:ZrO_2	−0.58	−0.39	1.049	0.970	1.444	2.523	2.152	118.7
	Ge:ZrO_2	−0.59	−0.49	1.040	0.969	1.466	2.524	2.141	118.9
	Sn:ZrO_2	−0.76	−1.24	1.007	0.970	1.642	2.740	2.075	123.1
	Pb:ZrO_2	unstable	−1.15	1.012	0.970	1.602	2.724	2.083	122.8
	Ti:ZrO_2	−0.73	−0.90	1.012	0.969	1.579	2.796	2.086	125.0
	Hf:ZrO_2	−0.80	−1.05	1.005	0.969	1.649	2.814	2.071	125.0
	Ce:ZrO_2	−0.86	−1.13	1.011	0.969	1.592	2.753	2.083	123.8

have been observed for CO adsorbed on CeO_2(100) surfaces, depending on the adsorption site;[55] the adsorption energies computed at the DFT level are between −0.42 and −0.51 eV, quite close to the value reported here. These are clear indications of the very local nature of the bonding of CO with Ce and with the other ions considered.

If the dopant is placed in the subsurface layer, then the effect on CO adsorption is indirect and not particularly pronounced. Only for Si and Ge one observes a small reduction in E_{ads} and virtually no shift in CO stretching frequency, Table 4.

To summarize, CO adsorption is only weakly affected by the presence of the dopant, with some effect observed for Ge and Ti ions segregated at the surface (however, we have shown above that these two ions prefer to occupy a subsurface site).

4.4. H_2O Adsorption. H_2O is produced in the decomposition reaction 6. Both molecular and dissociative H_2O adsorption have been considered, Table 5. On pure ZrO_2 water adsorbs in undissociated form with E_{ads} = −0.81 eV; a (probably small) barrier, not investigated here, separates this local minimum from the global minimum with E_{ads} = −1.01 eV consisting of a dissociated molecule where one proton is bound to a surface O, and an OH^- fragment is bound to a surface Zr ion, Figure 6. A distance of 1.61 Å separates the proton from the O atom of the OH group, see H1-O2 distance in Figure 6 and Table 5.

We consider first the case where the dopants are at the surface of zirconia. Here, molecular adsorption becomes unstable and local minima cannot be identified, with only two exceptions: Pb and Ce, Table 5. While for Pb, molecular adsorption is a local minimum, for Ce the order of stability is reversed with molecular adsorption being preferred over the dissociated form. The second interesting result is that in some cases the adsorption energy of dissociated water increases considerably compared to the pristine surface. In particular, this is the case of Si, Ge, and Ti where E_{ads} goes from −1.0 eV in pure ZrO_2 to −1.8 eV (Si) and − 2.1 eV (Ge), Table 5. For Sn, Pb, and Hf the adsorption energy is not too different from that of the pristine surface.

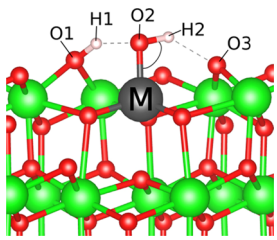

Figure 6. Structure of dissociated water on the surface of pristine and doped ZrO_2. M indicates the position of the dopant in M:ZrO_2.

Not surprisingly, the situation is rather different if the dopants are in subsurface sites. In this case the effect of the doping species is indirect, either related to some local structural rearrangement or to a local change in charge distribution. Si and Ge in subsurface sites reduce the overall binding strength and make H_2O molecular adsorption preferred, Table 5. Ti and Hf, with similar cation sizes to Zr, have little effect while Pb destabilizes the molecular adsorption mode which is no longer a local minimum in the region near the dopant. Of course, in other areas of the zirconia surface, unperturbed by the dopant, the situation becomes that of pure ZrO_2. Apart from the cases of Si and Ge, however, the overall adsorption energy of dissociated water is only moderately perturbed. The results are presented as graphs in Figure S6.

In the attempt to find a descriptor of the surface reactivity toward H_2O, we have plotted as shown in Figure S7 the dissociative adsorption energy versus the cation size, Figure S7a, and the distance of the proton of the OH group from a neighboring surface O ion (see the H2-O3 distance in Figure S7). While the data show a moderate correlation with the size of the dopant, there is a clear correlation with the strength of the hydrogen bond formed by the OH group, Figure S7b. The same analysis has been performed for subsurface dopants, again reporting the values of the dissociative adsorption. A better correlation is found with the cation size (R^2 = 0.88), Figure S7c and the other hydrogen bond formed by the dissociated water molecule that is between the H1 proton and the O2 atom of the OH group, see Figure 6 (R^2 = 0.90), Figure S7d).

4.5. H_2 Adsorption. The last reaction considered, reaction 7, consists in the decomposition of formic acid with formation of H_2 adsorbed on the ZrO_2 surface, and a CO_2 molecule that desorbs in the gas phase. H_2 adsorption on the t-ZrO_2 (101) surface results in a heterolytic dissociation of H_2 with formation of a proton, H^+, bound to a surface O^{2-} ion, and a hydride ion, H^-, bound to a surface Zr^{4+} ion, Figure 7.

https://dx.doi.org/10.1021/acscatal.0c04553
ACS Catal. 2021, 11, 554−567

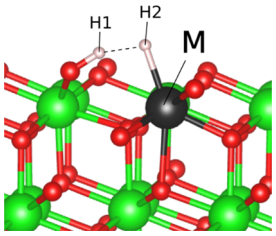

Figure 7. Structure of the dissociated H_2 molecule on the surface of pristine and doped ZrO_2. M indicates the position of the dopant in M:ZrO_2.

This process is favored compared to the homolytic dissociation, with two H^+ ions forming two surface OH^- groups, and two electrons transferred to Zr which changes its oxidation state from +4 to +3 ($4d^1$).[56] The occurrence of a heterolytic dissociation is consistent with the fact that zirconia is a nonreducible oxide.

This trend is confirmed by the results obtained with the present computational setup. On pure ZrO_2, the heterolytic dissociation of H_2 is moderately endothermic, $E_{ads}(H^+/H^-)$ = 0.32 eV, while the homolytic one is much higher in energy, $E_{ads}(H^+/H^+)$ = 2.63 eV. $E_{ads}(H^+/H^-)$ differs somewhat from our previous reported values, −0.06 eV;[56] the reason lies in the slightly different lattice parameters used (experimental in our previous study, fully optimized here). In fact, using the experimental lattice constants we reproduce the $E_{ads}(H^+/H^-)$ = −0.06 eV reported previously.[56] In the following study we will only consider the heterolytic H_2 dissociation; the role of homolytic splitting and its impact on the reducibility of the oxide will be considered in a future separate study.

Next, we have considered the same process but in the presence of a doping cation on the surface, Table 6. The results

Table 6. Adsorption Energy (E_{ads}, eV) and Bond Distances (R, Å) of H_2 Heterolytic Dissociative Adsorption on Pristine and Doped ZrO_2 Surfaces

H_2		E_{ads}	$R_{M...H2}$	$R_{H1...H2}$
	ZrO_2	0.32	1.968	1.382
surface	$Si:ZrO_2$	−0.59	1.482	1.975
	$Ge:ZrO_2$	−1.68	1.531	2.316
	$Sn:ZrO_2$	−0.87	1.728	1.877
	$Pb:ZrO_2$	−0.87	1.780	2.564
	$Ti:ZrO_2$	−0.41	1.742	1.467
	$Hf:ZrO_2$	0.25	1.928	1.341
	$Ce:ZrO_2$	unstable		
subsurface	$Si:ZrO_2$	0.80	2.020	1.180
	$Ge:ZrO_2$	0.72	2.002	1.236
	$Sn:ZrO_2$	0.14	1.963	1.441
	$Pb:ZrO_2$	0.20	1.968	1.403
	$Ti:ZrO_2$	0.43	1.974	1.366
	$Hf:ZrO_2$	0.32	1.961	1.438
	$Ce:ZrO_2$	0.20	1.966	1.401

are surprising. All the dopants, with the exception of Hf and Ce, lead to a change in the nature of the reaction, from slightly endothermic to exothermic. In some cases, such as Si, Sn, and Pb the effect is large, with energy gains that go from −0.59 to −0.87 eV; for Ge, the exothermicity is extremely large, −1.68 eV, Table 6. This has to do with a change in the nature of the interaction. When H is adsorbed on Zr, Ti, and Hf, the bonding has a similar nature, H has hydride character, and a direct H^+---H^- interaction is established that reflects in relatively short $R_{H1...H2}$ distances of about 1.4 Å, Table 6. When bound to Si, Ge, Sn, or Pb, a strong M-H bond with covalent character forms, which reflects in a short M-H distance and in a long $R_{H1...H2}$ distance, Table 6. This is a clear manifestation of the "orbital" contribution to the change in reactivity, as the tendency of group IV atoms to form covalent bonds changes both the reaction products and the bond strengths at the surface.

This effect is strictly related to the presence of the dopants on the surface layer. In fact, if the dopants are in subsurface positions, the effect on the dissociation reaction of H_2 is practically nonexisting except for Si and Ge that lead to an even more endothermic reaction, but there is no change in the sign of ΔE going from the pure to the doped surface, since now the main perturbation due to the dopants is of geometric instead of electronic nature.

In summary, of the four decomposition reactions considered, 4−7, the formation of an hydroxylated surface with desorption of CO_2 to the gas phase is the process that shows the strongest dependence on the presence of the surface dopants. In particular, dopants such as Si, Sn, and Pb, which prefer to stay on the top layer, can have disruptive consequences on the direction of the decomposition reaction, as it will be discussed below.

5. HCOOH DECOMPOSITION: THERMODYNAMICS

5.1. Undoped ZrO_2. Having considered the bonding modes of the various fragments in the previous sections, we can now look at the entire reaction profile, starting with pure zirconia, Table 7, where ΔE_R is reported for reactions 4−7, see

Table 7. Calculated Formic Acid Decomposition Energy (eV) on Pristine and Doped ZrO_2 Surfaces for H_2, H_2O, CO, and CO_2 Release (ΔE_R (H_2), ΔE_R (H_2O), ΔE_R (CO), and ΔE_R (CO_2), Respectively)[a]

		ΔE_R (H_2)[4]	ΔE_R (H_2O)[5]	ΔE_R (CO)[6]	ΔE_R (CO_2)[7]
	ZrO_2	−0.83	0.51	−0.08	0.57
surface	$Si:ZrO_2$	−0.52	0.41	−0.85	−0.34
	$Ge:ZrO_2$	−1.05	0.13	−1.17	−1.44
	$Sn:ZrO_2$	−0.81	0.70	−0.43	−0.62
	$Pb:ZrO_2$	−0.54	0.68	−0.10	−0.62
	$Ti:ZrO_2$	−1.21	0.27	−0.75	−0.17
	$Hf:ZrO_2$	−0.95	0.57	−0.23	0.49
	$Ce:ZrO_2$	−0.21	0.55	0.18	unstable
subsurface	$Si:ZrO_2$	−0.70	0.65	0.35	1.05
	$Ge:ZrO_2$	−0.60	0.66	0.34	0.97
	$Sn:ZrO_2$	−0.90	0.55	−0.32	0.38
	$Pb:ZrO_2$	−0.95	0.50	−0.22	0.44
	$Ti:ZrO_2$	−0.80	0.56	0.02	0.67
	$Hf:ZrO_2$	−0.78	0.52	−0.13	0.57
	$Ce:ZrO_2$	−0.97	0.49	−0.20	0.45

[a]the most stable isomers have been considered

above. A graphical representation is given in Figure 8. On undoped ZrO_2, the preferred process from an energy point of view is dehydrogenation, reaction 4, with a ΔE_R of −0.83 eV; dehydration, reaction 5, which is unfavorable in the gas phase, remains unfavorable also on the surface with a ΔE_R of 0.51 eV; decarbonylation, reaction 6 is exothermic but by −0.08 eV only. The loss of CO_2 with formation of a hydroxylated

https://dx.doi.org/10.1021/acscatal.0c04553
ACS Catal. 2021, 11, 554−567

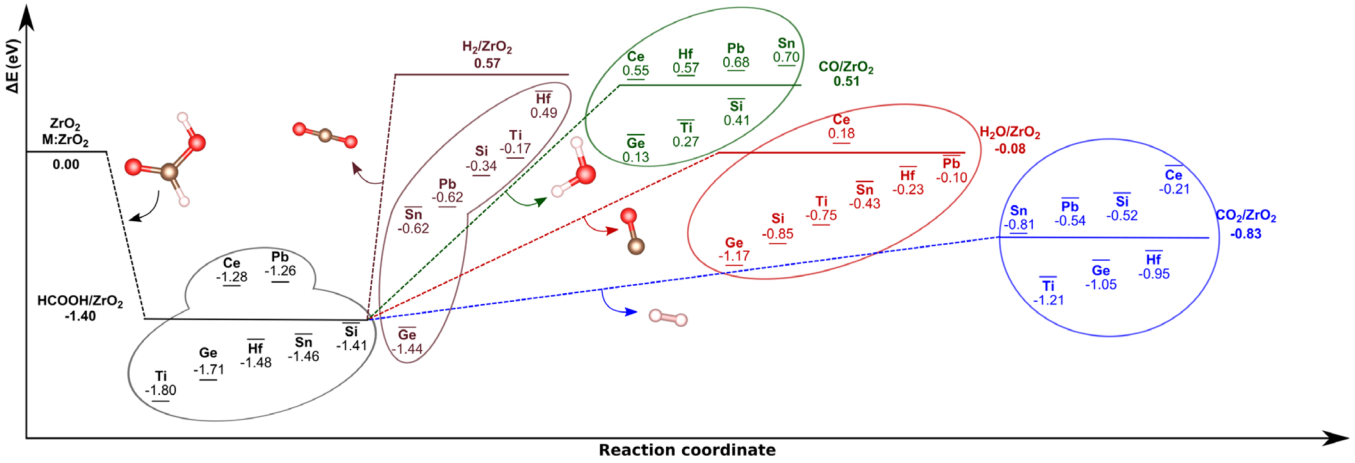

Figure 8. Energy profile for formic acid decomposition on the pristine and doped ZrO_2 surface (dopants in surface position). The adsorption energy of HCOOH is given for the most stable isomer together with ΔE_R (H_2) in blue, ΔE_R (CO) in red, ΔE_R (H_2O) in green, and ΔE_R (CO_2) in violet.

surface, reaction 7, is the least favorable process from an energy point of view with a ΔE_R of 0.57 eV.

So far, we have considered only energy contributions and neglected entropic terms. The adsorption enthalpy (ΔH) is defined approximately as the difference of total DFT energies of surface complexes and isolated species ($\Delta H \approx \Delta E$). On the other hand, Gibbs free energies can be calculated as $\Delta G^\circ = \Delta H - T(S_{ads} - S_g)$ for molecular adsorption and $\Delta G^\circ = \Delta H - T(S_g - S_{ads})$ for molecular desorption, where T is the absolute temperature and S_{ads} and S_g are the entropy of adsorbed and gas-phase molecules, respectively. Following the suggestion of Karlberg, Rossmeisl, and Nørskov,[57] S_{ads} can be neglected for small molecules such as CO, H_2O, H_2, and CO_2. The S_g of HCOOH, CO, H_2, CO_2, and H_2O are taken from a NIST database.[58] At 298 K, and 1 bar the TS_g contributions are: HCOOH 0.77 eV; CO 0.61 eV; H_2 0.40 eV; CO_2 0.66 eV; and H_2O 0.59 eV.

Using these values, we have constructed a new diagram, based on ΔG° values. This is shown for undoped ZrO_2 in Figure 9. The scenario, going from ΔH to ΔG° values, changes completely in terms of thermodynamic stabilities. The adsorption energy of $HCOOH_g$ on the ZrO_2 surface, ΔE = −1.40 eV, leads to a ΔG° = −0.63 eV when the loss of entropy of the gas-phase HCOOH species is taken into account. The decomposition of formic acid with release of H_2 is associated to a ΔG° = −1.23 eV once the entropy of gas-phase H_2 is included. This means that the reaction is downhill, Figure 9.

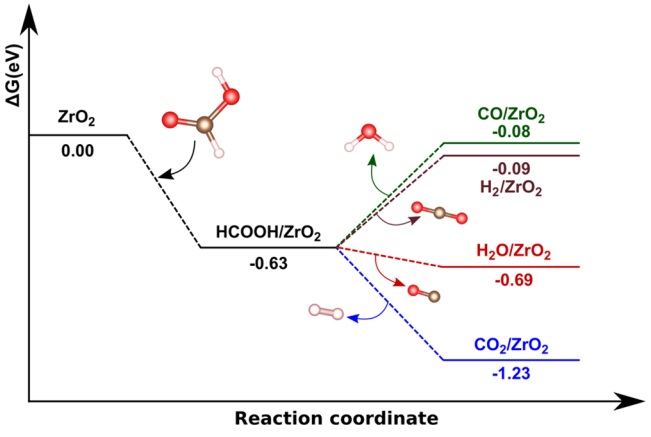

Figure 9. Gibbs free energy profile for formic acid decomposition on pristine ZrO_2. The adsorption free energy of HCOOH is given for the most stable isomer together with ΔG°_R (H_2) in blue, ΔG°_R (CO) in red, ΔG°_R (CO_2) in brown, and ΔG°_R (H_2O) in green.

Even the decomposition process with release of CO in the gas phase results in a ΔG° = −0.69 eV and a thermodynamically favorable reaction. The case of H_2O desorption remains almost thermoneutral, with a slightly negative ΔG° = −0.08 eV. Finally, for reaction 7 leading to CO_2 desorption, the effect of entropy is also that to make the reaction slightly favorable and similar to H_2O desorption, reaction 6. Thus, the inclusion of entropy has the effect of making the HCOOH decomposition more favorable in general but also to change the order of stability of the two least favorable processes, H_2O and CO_2 desorption. Since the entropy contribution is simply an additive term in our scheme, the effect of the dopants in terms of chemical activity can be discussed based on ΔE values only.

5.2. Doped ZrO_2. In this section we analyze the effect of the dopants. The results, Table 7, are summarized graphically in Figure 8. We start by considering Ti and Hf, the two metals belonging to the same group of Zr. These dopants prefer to be in subsurface sites, but the energy difference with surface sites is not large, about 0.2 eV, and it is possible that these dopants also occupy surface sites. Ti has the effect to reinforce the bonding of HCOOH to the surface (E_{ads} = −1.80 eV) but does not reverse the order of stability of the decomposition processes, with the dehydrogenation being preferred (ΔE_R = −1.21 eV), as for pure ZrO_2. The same applies to Hf that overall exhibits a very similar behavior to Zr with similar reaction energies, Figure 8. Next, we consider the behavior of Ce, the largest among the dopants considered. Ce has a moderate effect on the adsorption of HCOOH (E_{ads} = −1.28 eV) and makes all decomposition processes less favorable compared to undoped ZrO_2. This is because the large size of Ce, which leads to a clear preference for substitution in the top layer, results in weaker bonding of all the molecular fragments that originate from HCOOH decomposition. However, the order of preference of the four decomposition paths does not change. The main effect of Ce is to make the decomposition less favorable.

https://dx.doi.org/10.1021/acscatal.0c04553
ACS Catal. 2021, 11, 554−567

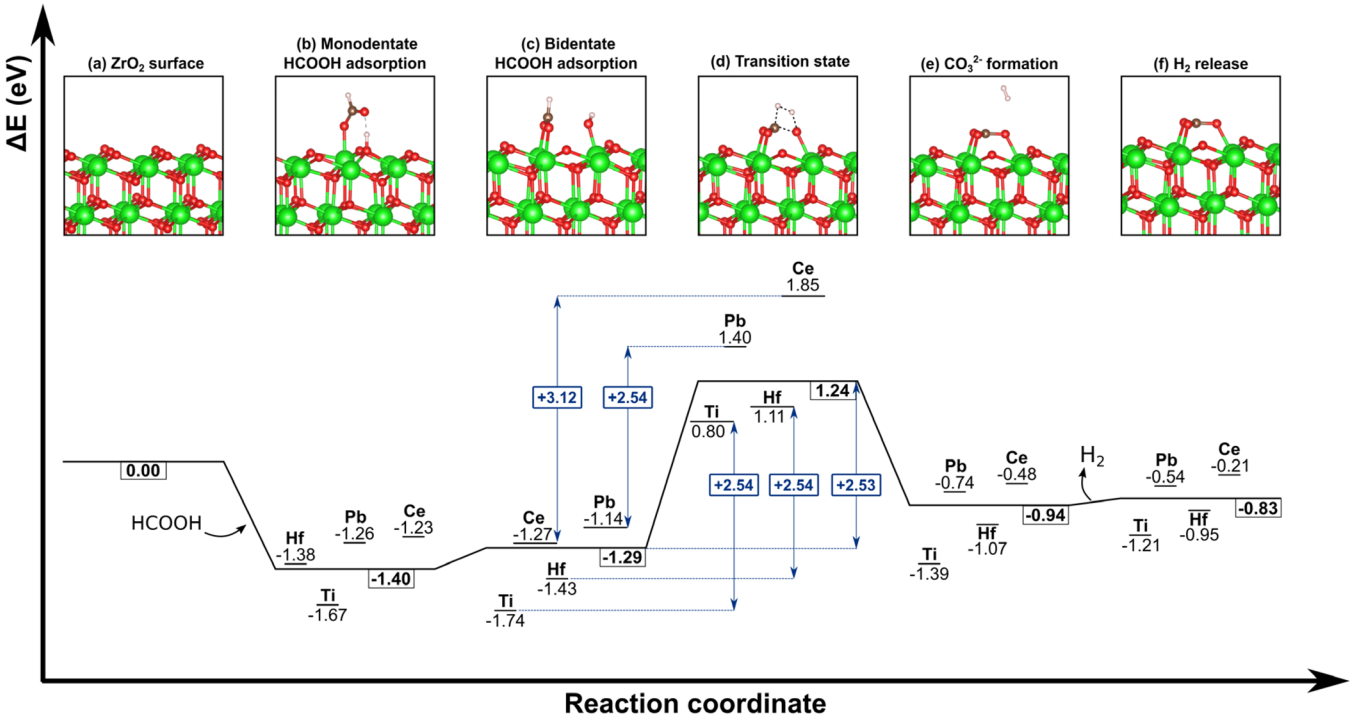

Figure 10. Energy profile with activation barrier for the dehydrogenation reaction of formic acid on the ZrO_2 surface and the effect of dopants in surface position.

Now we move to the analysis of the effect of the four dopants belonging to group IV, Si, Ge, Sn, and Pb, in this order. They all prefer to occupy surface sites, with the exception of Ge that preferentially replaces Zr in subsurface sites, Figure 1. Si has virtually no effect on HCOOH adsorption, with E_{ads} = −1.41 eV, practically the same as the undoped system. On the contrary, very different are the consequences on HCOOH decomposition. In fact, dehydrogenation, (ΔE_R = −0.52 eV) is no longer the preferred process. Decarbonylation, with formation of a hydroxylated surface, is the preferred path, with ΔE_R = −0.85 eV, followed by CO_2 desorption, ΔE_R = −0.34 eV, and dehydration, ΔE_R = 0.41 eV. Therefore, Si dopants locally lead to a different decomposition mechanism. It should be mentioned, however, that the reaction on regular Zr sites occurs with a similar ΔE_R = −0.83 eV, Figure 8, so that if the concentration of the Si dopants is low, their effect on the HCOOH decomposition will be limited.

As we mentioned, Ge does not occupy preferentially surface sites, Figure 1. If this occurs, however, the effect on the reaction is dramatic. HCOOH adsorption is only moderately affected, with E_{ads} = −1.71 eV, but the sequence of the decomposition reactions is completely changed. Now the loss of CO_2, reaction 7, is by far the most favorable process, with ΔE_R = −1.44 eV, followed by decarbonylation, reaction 5, with ΔE_R = −1.17 eV, dehydrogenation, reaction 1, with ΔE_R = −1.05 eV, and finally by dehydration, ΔE_R = 0.13 eV. The very different bond strengths of surface Ge atoms with some of the fragments generated in HCOOH decomposition, H atoms in particular, is at the origin of this complete change of reactivity.

Sn does not alter the adsorption properties of HCOOH, E_{ads} = −1.46 eV. It also does not affect the dehydrogenation process, which with ΔE_R = −0.81 eV remains energetically preferred and also very similar to pure ZrO_2 in terms of exothermicity. Some effect of Sn is seen on the other reactions, since CO_2 desorption (ΔE_R = −0.62 eV) is now the next most favorable process after H_2 desorption, at variance with the undoped surface. This is followed by decarbonylation and dehydration, Figure 8. The last case is that of Pb. Pb has the effect of reducing slightly the adsorption energy of HCOOH, E_{ads} = −1.26 eV, but also to change the order of preference of the decomposition processes: the lowest energy is associated to reaction 7, CO_2 desorption (ΔE_R = −0.62 eV) which is slightly favorable compared to dehydrogenation, reaction 4 (ΔE_R = −0.54 eV). The other two processes are clearly less favorable. However, while Pb has the effect to change the reactivity, the overall exothermicity of HCOOH decomposition is higher for the undoped surface (ΔE_R = −0.83 eV) so that as for the case of Si, the reaction will occur preferentially in regions of the surface not affected by the presence of the dopant.

So far, we have discussed the case of dopants occupying surface sites. In Table 7 we report also the energetics for the same dopants in subsurface sites. From this table it is apparent that the chemistry of the surface ions is barely affected by the presence of the dopants in the subsurface. Dehydrogenation remains clearly preferred, with ΔE_R that goes from −0.60 eV for Ge to −0.97 eV for Ce, two values that are slightly above and slightly below that found for the undoped surface, −0.83 eV, Table 7.

6. HCOOH DECOMPOSITION: KINETICS

Finally, we have considered the dopant effect on the barrier for the dehydrogenation reaction 1, which, according to the results presented in previous sections, is the most favorable for ZrO_2 and for many of the dopants considered. The reaction path is shown in Figure 10. The first step consists in the adsorption of HCOOH with formation of a monodentate formate ion, Figure 4a. This is then transformed into a bidentate isomer which has the proper orientation to react with a surface OH group and lead to the final product, CO_2(ads) + H_2(g). This isomer has a slightly different orientation compared to that

https://dx.doi.org/10.1021/acscatal.0c04553
ACS Catal. 2021, 11, 554−567

reported in Figure 4b. From this precursor, the formation of a flat lying CO_3^{2-} unit and a hydrogen molecule (obtained by combining one H atom from the C−H group and the other one from the O−H group), occurs via a transition state. The associated barrier is relatively high, being about 2.5 eV for undoped ZrO_2, Figure 10. Doping has a negligible effect on the barriers, see Figure 10. In the case of Ce, we even found an increase of the barrier, from 2.5 to 3.1 eV, while the presence of the other dopants has virtually no effect. This allows us to conclude that while some dopants have an effect on the thermodynamics of the process, the kinetics is not affected.

These results have been obtained assuming that the surface OH group, which forms from the dissociative adsorption of HCOOH is bound to a Zr ion, while the surface dopant is involved in bonding the $HCOO^-$ unit, Figure 4. Another possibility is that the $HCOO^-$ fragment is bound to an undoped region of the surface, while the OH unit forms adjacent to a cation dopant. This situation has been analyzed for the case of Ti and Ce, see Figure S8. For the case of Ti, we observe that the precursor state where HCOOH is dissociated is more stable in the new configuration, Figure S8a, E_{ads} = −2.10 eV (to be compared with −1.80 eV of the former configuration, Table 2) but this results in a larger barrier, 2.92 eV. With Ce, the precursor state is considerably destabilized, from −1.28 to −0.78 eV, and the barrier is reduced from 3.12 to 2.63 eV. Overall, exchanging the position of the dopants has obviously an impact on the adsorption energies but does not result in major changes in the conclusions.

7. CONCLUSIONS

In this work, we have studied systematically the effect of isovalent dopants on the chemical reactivity of ZrO_2 in a particular surface process, the decomposition of formic acid. The adsorption of HCOOH on the surface of zirconia can give rise to four different decomposition paths, with (a) release in the gas phase of a H_2 molecule, leaving behind a surface carbonate (adsorbed CO_2), (b) CO desorption, with formation of an adsorbed water molecule and of an hydroxylated surface, (c) release of H_2O, with CO being the fragment that remains adsorbed on the surface, or (d) CO_2 desorption leaving on the surface a dissociated H_2 molecule. On the undoped ZrO_2 surface release of H_2 is the preferred reaction, with a highly favorable process (ΔG° = −1.23 eV). This is followed by decarbonylation (ΔG° = −0.69 eV), CO_2 desorption (ΔG° = −0.09 eV), and the loss of water (ΔG° = −0.08 eV).

The effect of tetravalent dopants has been considered by replacing Zr ions in various positions of the solid: bulk, subsurface, and surface. All the dopants considered prefer to occupy surface or subsurface sites. In particular, Si, Sn, Ce, and Pb prefer to replace Zr ions at the surface, while Ti, Ge, and Hf prefer to go subsurface. This is related to a combination of size of the doping ion, tendency to assume specific coordination numbers, and the cost to rearrange the structure to accommodate the dopant. Introducing dopants in an oxide material can be done in various ways, but in general with little control on the final position taken by the dopant. If the synthesis is done under conditions of thermodynamic equilibrium, the dopants will assume the most favorable position. However, dopants can occupy different positions depending on the external conditions of the synthesis. If the dopants are more stable in surface or subsurface positions, then a higher concentration of these species could be obtained by promoting migration under strong thermal annealing conditions.

The dopants modify the electronic structure of the solid: while they have a modest effect on the position of the top of the O 2p valence band, hence on the basic properties of the surface O ions, some dopants induce a change in the position of the bottom of the conduction band, thus modifying the band gap. More relevant is the fact that several dopants (a) induce locally structural modification and (b) introduce new empty orbitals available for the interaction with the adsorbed species. Ge introduces energy levels just below the bottom of the conduction band, while Ti and Sn introduce impurity levels deep in the gap. The presence of low-lying acceptor states in the gap becomes even more pronounced with Pb and Ce. This is expected to locally affect the Lewis acid properties of the surface.

The HCOOH decomposition reaction has been considered, and to this end the nature of adsorbed HCOOH, CO_2, H_2O, CO, and H_2 molecules has been studied as a function of doping. Since the entropy contribution of adsorption and desorption of gas-phase species is independent of the dopant, the effect of doping can be discussed based on ΔE values only.

Ti and Hf do not reverse the order of preference of the four reactions and exhibit a similar behavior to Zr. Ce, due to the large size, makes all decomposition processes less favorable compared to the undoped ZrO_2. More interesting is the role of group IV dopants, Si, Ge, Sn, and Pb that prefer to occupy surface sites, with the exception of Ge. In the presence of Si, dehydrogenation is no longer the preferred process and decarbonylation, with formation of a hydroxylated surface, becomes the preferred path followed by CO_2 desorption and dehydration. Therefore, Si dopants induce locally a different decomposition mechanism. If Ge occupies surface sites, its effect on the reaction is dramatic since the loss of CO_2, reaction 7, becomes by far the most favorable process followed by decarbonylation and dehydrogenation. With Sn, on the other hand, dehydrogenation remains energetically preferred but the ordering of the other reactions is modified. The last case is that of Pb which changes the order of preference of the decomposition processes, with CO_2 desorption slightly preferred over dehydrogenation. These effects virtually disappear when the dopants occupy subsurface sites.

In summary, we have shown that the presence of isolated, highly diluted, isovalent dopants on the surface of ZrO_2 can have important consequences on the electronic structure and on the chemical reactivity. This depends specifically on the dopant and on the modifications induced on the surrounding. Sometimes dopants in oxides are referred to as single atom catalysts, at least when these correspond to atomic species incorporated in a supporting matrix. This work shows that important changes occur in the local reactivity of the surface even without changing the total electron density available at a given active site. The changes in reactivity are determined by structural changes in the local environment, “steric effects”, or by a different energy of the atomic states involved, “orbital effect”. The combination of steric and orbital effects determines the modified surface reactivity even without the occurrence of important electron transfer processes as for transition metal-based single atom catalysts.

https://dx.doi.org/10.1021/acscatal.0c04553
ACS Catal. 2021, 11, 554−567

■ ASSOCIATED CONTENT

Supporting Information

The Supporting Information is available free of charge at https://pubs.acs.org/doi/10.1021/acscatal.0c04553.

Density of states, graphic representation of adsorption energies, and correlation diagrams (PDF)

■ AUTHOR INFORMATION

Corresponding Author

Gianfranco Pacchioni − *Dipartimento di Scienza dei Materiali, Universitá di Milano-Bicocca, 20125 Milano, Italy;* orcid.org/0000-0002-4749-0751; Email: Gianfranco.pacchioni@unimib.it

Author

Farahnaz Maleki − *Dipartimento di Scienza dei Materiali, Universitá di Milano-Bicocca, 20125 Milano, Italy;* orcid.org/0000-0002-5747-1319

Complete contact information is available at: https://pubs.acs.org/10.1021/acscatal.0c04553

Notes

The authors declare no competing financial interest.

■ ACKNOWLEDGMENTS

This work was supported by the Italian Ministry of University and Research (MIUR) through the PRIN Project 20179337R7, and the grant Dipartimenti di Eccellenza - 2017 "Materials For Energy". Support from the COST Action 18234 is also gratefully acknowledged. The work is supported also by the Australian Research Council under the Discovery Project Grant DP 200100313.

■ REFERENCES

(1) Wang, W.; Tadé, M. O.; Shao, Z. Nitrogen-doped simple and complex oxides for photocatalysis: a review. *Prog. Mater. Sci.* **2018**, *92*, 33−63.

(2) McFarland, E. W.; Metiu, H. Catalysis by doped oxides. *Chem. Rev.* **2012**, *113*, 4391−4427.

(3) Sun, Y. F.; Liu, S. B.; Meng, F. L.; Liu, J. Y.; Jin, Z.; Kong, L. T.; Liu, J. H. Metal oxide nanostructures and their gas sensing properties: a review. *Sensors* **2012**, *12*, 2610−2631.

(4) Dey, A. Semiconductor metal oxide gas sensors: A review. *Mat. Sci. Eng. B* **2018**, *229*, 206−217.

(5) Di Valentin, C.; Pacchioni, G. Spectroscopic properties of doped and defective semiconducting oxides from hybrid density functional calculations. *Acc. Chem. Res.* **2014**, *47*, 3233−3241.

(6) Fabbri, E.; Pergolesi, D.; Traversa, E. Materials challenges toward proton-conducting oxide fuel cells: a critical review. *Chem. Soc. Rev.* **2010**, *39*, 4355−4369.

(7) Ricca, C.; Ringuedé, A.; Cassir, M.; Adamo, C.; Labat, F. Revealing the properties of the cubic ZrO_2 (111) surface by periodic DFT calculations: reducibility and stabilization through doping with aliovalent Y_2O_3. *RSC Adv.* **2015**, *5*, 13941−13951.

(8) Pala, R. G. S.; Metiu, H. Modification of the oxidative power of ZnO (1010) surface by substituting some surface Zn atoms with other metals. *J. Phys. Chem. C* **2007**, *111*, 8617−8622.

(9) Tsvetkov, N.; Lu, Q.; Sun, L.; Crumlin, E. J.; Yildiz, B. Improved chemical and electrochemical stability of perovskite oxides with less reducible cations at the surface. *Nat. Mater.* **2016**, *15*, 1010−1016.

(10) Stavale, F.; Shao, X.; Nilius, N.; Freund, H. J.; Prada, S.; Giordano, L.; Pacchioni, G. Donor characteristics of transition-metal-doped oxides: Cr-doped MgO versus Mo-doped CaO. *J. Am. Chem. Soc.* **2012**, *134*, 11380−11383.

(11) Liu, W. C.; Wu, D.; Li, A. D.; Ling, H. Q.; Tang, Y. F.; Ming, N. B. Annealing and doping effects on structure and optical properties of sol−gel derived ZrO_2 thin films. *Appl. Surf. Sci.* **2002**, *191*, 181−187.

(12) Ji, P.; Mao, Z.; Wang, Z.; Xue, X.; Zhang, Y.; Lv, J.; Shi, X. Improved surface-enhanced Raman scattering properties of ZrO_2 nanoparticles by Zn doping. *Nanomaterials* **2019**, *9*, 983.

(13) Kuryliszyn-Kudelska, I.; Arciszewska, M.; Małolepszy, A.; Mazurkiewicz, M.; Stobinski, L.; Grabias, A.; Kopcewicz, M.; Paszkowicz, W.; Minikaev, R.; Domukhovski, V.; Nedelko, N.; Dobrowolski, W. Influence of Fe doping on magnetic properties of ZrO_2 nanocrystals. *J. Alloy. Compd.* **2015**, *632*, 609−616.

(14) Tiwari, N.; Kuraria, R. K.; Tamrakar, R. K. Thermoluminescence glow curve for UV induced ZrO_2: Ti phosphor with variable concentration of dopant and various heating rate. *J. Radiat. Res. Appl. Sci.* **2019**, *7*, 542−549.

(15) Gnanamoorthi, K.; Balakrishnan, M.; Mariappan, R.; Kumar, E. R. Effect of Ce doping on microstructural, morphological and optical properties of ZrO_2 nanoparticles. *Mater. Sci. Semicond. Process.* **2015**, *30*, 518−526.

(16) Ravichandran, A. T.; Pushpa, K. C. S.; Ravichandran, K.; Karthika, K.; Nagabhushana, B. M.; Mantha, S.; Swaminathan, K. Effect of Al doping on the structural and optical properties of ZrO_2 nanopowders synthesized using solution combustion method. *Superlattices Microstruct.* **2014**, *75*, 533−542.

(17) Gionco, C.; Livraghi, S.; Maurelli, S.; Giamello, E.; Tosoni, S.; Di Valentin, C.; Pacchioni, G. Al-and Ga-doped TiO_2, ZrO_2, and HfO_2: the nature of O 2p trapped holes from a combined electron paramagnetic resonance (EPR) and density functional theory (DFT) study. *Chem. Mater.* **2015**, *27*, 3936−3945.

(18) Wang, A.; Li, J.; Zhang, T. Heterogeneous single-atom catalysis. *Nat. Rev. Chem.* **2018**, *2*, 65−81.

(19) De Rita, L.; Resasco, J.; Dai, S.; Boubnov, A.; Thang, H. V.; Hoffman, A. S.; Ro, I.; Graham, G. W.; Bare, S. R.; Pacchioni, G.; Pan, X.; Christopher, P. Structural evolution of atomically dispersed Pt catalysts dictates reactivity. *Nat. Mater.* **2019**, *18*, 746−751.

(20) Polierer, S.; Jelic, J.; Pitter, S.; Studt, F. On the reactivity of the Cu/ZrO_2 system for the hydrogenation of CO_2 to methanol: A density functional theory study. *J. Phys. Chem. C* **2019**, *123*, 26904−26911.

(21) Zhang, Z.; Zhang, L.; Hülsey, M. J.; Yan, N. Zirconia phase effect in Pd/ZrO_2 catalyzed CO_2 hydrogenation into formate. *Mol. Catal.* **2019**, *475*, 110461.

(22) Ma, Y.; Wang, J.; Goodman, K. R.; Head, A. R.; Tong, X.; Stacchiola, D. J.; White, M. G. Reactivity of a zirconia-copper inverse catalyst for CO_2 hydrogenation. *J. Phys. Chem. C* **2020**, *124*, 22158−22172.

(23) Yin, K.; Shen, Y. Theoretical Insights into CO_2 hydrogenation to HCOOH over $Fe_xZr_{1-x}O_2$ solid solution catalyst. *Appl. Surf. Sci.* **2020**, *528*, 146926.

(24) Luo, Q.; Beller, M.; Jiao, H. Formic acid dehydrogenation on surfaces: a review of computational aspect. *J. Theor. Comput. Chem.* **2013**, *12*, 1330001.

(25) Uemura, Y.; Taniike, T.; Tada, M.; Morikawa, Y.; Iwasawa, Y. Switchover of reaction mechanism for the catalytic decomposition of HCOOH on a TiO_2 (110) surface. *J. Phys. Chem. C* **2007**, *111*, 16379−16386.

(26) Yoshimoto, M.; Takagi, S.; Umemura, Y.; Hada, M.; Nakatsuji, H. Theoretical study on the decomposition of HCOOH on a ZnO (1010) surface. *J. Catal.* **1998**, *173*, 53−63.

(27) Lintuluoto, M.; Nakatsuji, H.; Hada, M.; Kanai, H. Theoretical study of the decomposition of HCOOH on an MgO (100) surface. *Surf. Sci.* **1999**, *429*, 133−142.

(28) Avdeev, V. I.; Parmon, V. N. Molecular mechanism of the formic acid decomposition on V_2O_5/TiO_2 catalysts: a periodic DFT analysis. *J. Phys. Chem. C* **2011**, *115*, 21755−21762.

(29) Lee, H. J.; Kang, D. C.; Pyen, S. H.; Shin, M.; Suh, Y. W.; Han, H.; Shin, C. H. Production of H_2-free CO by decomposition of formic acid over ZrO_2 catalysts. *Appl. Catal. A Gen.* **2017**, *531*, 13−20.

(30) Kresse, G.; Furthmüller, J. Efficiency of ab-initio total energy calculations for metals and semiconductors using a plane wave basis set. *Comput. Mater. Sci.* **1996**, *6*, 15−50.
(31) Kresse, G.; Hafner, J. Ab initio molecular dynamics for liquid metals. *Phys. Rev. B: Condens. Matter Mater. Phys.* **1993**, *47*, 558.
(32) Kresse, G.; Hafner, J. ab initio molecular-dynamics simulation of the liquid-metal−amorphous-semiconductor transition in germanium. *Phys. Rev. B: Condens. Matter Mater. Phys.* **1994**, *49*, 14251.
(33) Perdew, J. P.; Burke, K.; Ernzerhof, M. Generalized gradient approximation made simple. *Phys. Rev. Lett.* **1996**, *77*, 3865.
(34) Anisimov, V. I.; Zaanen, J.; Andersen, O. K. Band theory and Mott insulators: Hubbard U instead of stoner I. *Phys. Rev. B: Condens. Matter Mater. Phys.* **1991**, *44*, 943.
(35) Dudarev, S.; Botton, G.; Savrasov, S.; Humphreys, C.; Sutton, A. Electron-energy-loss spectra and the structural stability of nickel oxide: An LSDA+U study. *Phys. Rev. B: Condens. Matter Mater. Phys.* **1998**, *57*, 1505.
(36) Di Liberto, G.; Pifferi, V.; Lo Presti, L.; Ceotto, M.; Falciola, L. Atomistic explanation for interlayer charge transfer in metal−semiconductor nanocomposites: the Ccase of silver and anatase. *J. Phys. Chem. Lett.* **2017**, *8*, 5372−5377.
(37) Puigdollers, A. R.; Illas, F.; Pacchioni, G. Structure and properties of zirconia nanoparticles from density functional theory calculations. *J. Phys. Chem. C* **2016**, *120*, 4392−4402.
(38) Ciftci, Y. O.; Ergun, A. H.; Colakoglu, K.; Deligoz, E. First principles LDA+U and GGA+U study of HfO_2: Dependence on the effective U parameter. *GU J. Sci.* **2007**, *75*, 627−636.
(39) Livraghi, S.; Paganini, M. C.; Giamello, E.; Di Liberto, G.; Tosoni, S.; Pacchioni, G. Formation of reversible adducts by adsorption of oxygen on Ce−ZrO_2: An unusual η^2 ionic superoxide. *J. Phys. Chem. C* **2019**, *123*, 27088−27096.
(40) Capdevila-Cortada, M.; Łodziana, Z.; López, N. Performance of DFT+ U approaches in the study of catalytic materials. *ACS Catal.* **2016**, *6*, 8370−8379.
(41) Grimme, S.; Ehrlich, S.; Goerigk, L. Effect of the damping function in dispersion corrected density functional theory. *J. Comput. Chem.* **2011**, *32*, 1456−1465.
(42) Grimme, S.; Antony, J.; Ehrlich, S.; Krieg, H. A Consistent and accurate ab initio parametrization of density functional dispersion correction (DFT-D) for the 94 elements H-Pu. *J. Chem. Phys.* **2010**, *132*, 154104.
(43) Blöchl, P. E. Projector augmented-wave method. *Phys. Rev. B: Condens. Matter Mater. Phys.* **1994**, *50*, 17953.
(44) Kresse, G.; Joubert, D. From ultrasoft pseudopotentials to the projector augmented-wave method. *Phys. Rev. B: Condens. Matter Mater. Phys.* **1999**, *59*, 1758.
(45) Maleki, F.; Pacchioni, G. DFT study of ^{17}O NMR spectroscopy applied to zirconia surfaces and nanoparticles. *J. Phys. Chem. C* **2019**, *123*, 21629−21638.
(46) Henkelman, G. B.; Uberuaga, P. H.; Jónsson, H. A climbing image nudged elastic band method for finding saddle points and minimum energy paths. *J. Chem. Phys.* **2000**, *113*, 9901−9904.
(47) Gionco, C.; Paganini, M. C.; Giamello, E.; Burgess, R.; Di Valentin, C.; Pacchioni, G. Paramagnetic defects in polycrystalline zirconia: an EPR and DFT study. *Chem. Mater.* **2013**, *25*, 2243−2253.
(48) Gionco, C.; Paganini, M. C.; Giamello, E.; Burgess, R.; Di Valentin, C.; Pacchioni, G. Cerium-doped zirconium dioxide, a visible-light-sensitive photoactive material of third generation. *J. Phys. Chem. Lett.* **2014**, *5*, 447−451.
(49) Ignatchenko, A. V. Density functional theory study of carboxylic acids adsorption and enolization on monoclinic zirconia surfaces. *J. Phys. Chem. C* **2011**, *115*, 16012−16018.
(50) Pacchioni, G. Ketonization of carboxylic acids in biomass conversion over TiO_2 and ZrO_2 surfaces: a DFT perspective. *ACS Catal.* **2014**, *4*, 2874−2888.
(51) Chen, H. Y. T.; Tosoni, S.; Pacchioni, G. A DFT study of the acid−base properties of anatase TiO_2 and tetragonal ZrO_2 by adsorption of CO and CO_2 probe molecules. *Surf. Sci.* **2016**, *652*, 163−171.
(52) Roth, J. P.; Pacchioni, G. Influence of strain on acid−basic properties of oxide surfaces. *J. Phys. Chem. C* **2020**, *124*, 19126−19135.
(53) Bolis, V.; Morterra, C.; Fubini, B.; Ugliengo, P.; Garrone, E. Temkin-type model for the description of induced heterogeneity: CO adsorption on group 4 transition metal dioxides. *Langmuir* **1993**, *9*, 1521−1528.
(54) Adamo, C.; Lelj, F. A hybrid density functional study of the first-row transition-metal monocarbonyls. *J. Chem. Phys.* **1995**, *103*, 10605−10613.
(55) Yang, C.; Capdevila-Cortada, M.; Dong, C.; Zhou, Y.; Wang, J.; Yu, X.; Nefedov, A.; Heißler, S.; López, N.; Shen, W.; Wöll, C.; Wang, Y. Surface Refaceting Mechanism on Cubic Ceria. *J. Phys. Chem. Lett.* **2020**, *11*, 7925−7931.
(56) Ruiz Puigdollers, A.; Tosoni, S.; Pacchioni, G. Turning a nonreducible into a reducible oxide via nanostructuring: opposite behavior of bulk ZrO_2 and ZrO_2 nanoparticles towards H_2 adsorption. *J. Phys. Chem. C* **2016**, *120*, 15329−15337.
(57) Karlberg, G. S.; Rossmeisl, J.; Nørskov, J. K. Estimation of electric field effects on the oxygen reduction reaction based on the density functional theory. *Phys. Chem. Chem. Phys.* **2007**, *9*, 5158−6161.
(58) https://webbook.nist.gov.

https://dx.doi.org/10.1021/acscatal.0c04553
ACS Catal. 2021, 11, 554−567